www.sciencemag.org/content/363/6423/187/suppl/DC1

Supplementary Materials for

Cell-autonomous clock of astrocytes drives circadian behavior in mammals

Marco Brancaccio*, Mathew D. Edwards, Andrew P. Patton, Nicola J. Smyllie, Johanna E. Chesham, Elizabeth S. Maywood, Michael H. Hastings*

*Corresponding author. Email: m.brancaccio@imperial.ac.uk (M.B.); mha@mrc-lmb.cam.ac.uk (M.H.H.)

Published 11 January 2019, *Science* **363**, 187 (2019)
DOI: 10.1126/science.aat4104

This PDF file includes:

Other Supplementary Materials for this manuscript include the following:
(available at www.sciencemag.org/content/363/6423/187/suppl/DC1)

Movies S1 and S2 (.mov)

Materials and Methods

Mice

All animal work was conducted and licensed in accordance with the Code of Practice for the Housing and Care of Animals Bred, Supplied or Used for Scientific Purposes under A(SP)A and the EU Directive 2010/63/EU, and with local ethical approval (MRC-LMB AWERB). All the experiments were performed on healthy mice, with normal immune status, housed in a specific pathogen free (SPF) unit (Ares Facility, Babraham Institute Campus, Cambridge, UK). Per2::Luc mice (allele: B6.129S6-Per2tm1Jt/J) were gifted by Joe Takahashi (UT Southwestern, US). Cry1/2-null mice were gifted by G. T. van der Horst (Department of Genetics, Erasmus MC, Rotterdam, The Netherlands). All lines were maintained on a C57BL/6J background.

AAV particles design and production

Plasmids encoding for *Cry1*-Flex-Cry1-Luc and *Cry1*-Flex-Cry1::EGFP were produced in-house. Briefly, the Cry1 promoter was PCR-amplified from *mCry1*-Cry1::EGFP (25) using the following primers: Fwd: CATACGCGTCAGAACTATGCCTCCTCCC, Rev: CAGTCTAGAGTCGACTGCAGAATTCGAAG and then cloned into pAAV-EF1a-DIO-Chr2(H113R)-EYFP-WPRE-HGHpA (Addgene 20298) by using MluI and EcoRI sites. The resulting plasmid AAV-pCry1-DIO-ChR2-YFP was then used to produce both mCry1-Luc and mCry1-Cry1::EGFP. Luc ORF was PCR-amplified from pGL3 using: Fwd: CATGCTAGCTCATGGAAGACGCCAAAA and Rev: CATGGCGCGCCTTACACGGCGATCTTTCCGC, whereas Cry1::EGFP amplified from *Cry1*-Cry1::EGFP using: Fwd: CATGCTAGCGTTTAAACTTAAGCTTCGAATTCTG and Rev: CATGGCGCGCCCTATTACTTGTACAGCTCGTCC. Both ‘Luc' or 'Cry1::EGFP’ PCR fragments were then cloned into AAV-pCry1-DIO-ChR2-YFP by using AscI and NheI sites. After confirmation of ITR integrity by SmaI digest, plasmids were packaged into AAVs by Penn Vector Core (University of Pennsylvania). AAVs encoding Syn-RCaMP1h, Syn-GCaMP3, Syn-iGluSnFR (Loren L. Looger and the HHMI Janelia Farm Research Campus) and GFAP-EGFP were purchased from Penn Vector Core. AAVs encoding for GFAP-mCherry::Cre and Syn-mCherry:Cre (*3*) were purchased from Gene Therapy Center Vector Core (University of North Carolina).

AAV transduction and multi-channel live imaging of SCN slices

SCN organotypic cultures from p12-p14 pups were obtained, cultured and transduced with AAV viral particles as previously described (*9*). SCN slices were cultured in medium containing 100 µM luciferin (Biosynth) for bioluminescence detection, which was detected by continuous photon multiplier tube recording (PMT) (Hamamatsu) (cpm= counts per minute) **(Fig. 1G to I, Fig. 4 C and D, Fig. 4 G to J)**, or by LV200 imaging (Olympus Microscopy, UK) (**Fig. 1B to F, Fig. 3, 4E and F)**. Multi-channel bioluminescence/fluorescence imaging was generally performed as previously described (*9*) using the LV200 systems equipped with EM-CCD camera (Hamamatsu). Exposure varied between 200-600 ms for fluorescent reporters, bioluminescence signal was acquired over 30 min. Time resolution is 30 minutes for all the reporters used. Time-series were downloaded as grey-scale image stacks and pre-processed in ImageJ (NIH). A false color LUT was imposed to each channel and the different channels assembled as composite multi-channel stacks, de-speckled and ROI normalized to subtract background. For experiments assessing live dynamics of neuronal and astrocytic Cry1 expression **(Fig. 3)**, SCN slices from Cry1/2-

null mice expressing Per2::Luc were transduced with *Cry1*-Flexed-Cry1::EGFP AAVs (2µl) a week after dissection. On confirmation of absence of detectable oscillations by PMT recording (~7 days of recording), medium was changed and AAVs encoding GFAP-mCherry::Cre and Syn-mCherry::Cre (1.5µl) (*3*) were added. Slices were immediately transferred to LV200 stage for uninterrupted bioluminescence/fluorescence live recording (~14 days), without further medium changes. For neuronal calcium detection in SCN explants in which Cry1 expression was expressed in astrocytes **(Fig. 4)**, medium was changed and slices were super-transduced with Syn-RCaMP1h (1.5µl) expressing AAVs (*3*). For SCN spatial phase-mapping of Syn-RCaMP1h signals **(Fig. 4D)** an ImageJ grid map macro (designed in-house by A.P.P.) was applied onto the SCN space, as defined by anatomical landmarks (third ventricle-top, optic chiasm-bottom) to determine phase values in space. ROIs were 8X8 pixel squares in all the experiments. A single SCN from three independent biological replicates was used to perform this analysis in Cry1-complemented Cry1/2-null and WT mice. Values along the y-axis were used to parcel the SCN space in four equal quadrants and ROIs phase values from the top and bottom quadrants used to calculate dorsal and ventral average phases. Data were then normalized to their respective dorsal values to quantify Δ phase within groups (biological replicates) and across groups (Cry1-complemented Cry1/2-null vs WT mice).

In vivo Cry1 complementation experiments

Wheel-running behavior of individually caged (8-16 weeks old) Cry1/2-null male mice kept was recorded in light-tight chambers with food and water provided ad libitum. Mice were kept for at least 7 days in a 12:12 LD schedule (LD1), before being released in constant red dim light (DD1) for >10 days. AAV mixes (500nl/injection site composed of *Cry1*-Flex-Cry1::EGFP (250nl) and GFAP-mCherry::Cre (250nl) (Cre-treated group), or GFAP-EGFP (250nl) (control group) respectively were bilaterally injected with a stereotaxic frame (KOPF Instruments) by using the following coordinates to bregma point (medio-lateral ±0.2mm, anterior-posterior 0.0 mm, dorsal-ventral 5.5 mm), under halothane anaesthesia. Mice were left in 12:12 LD conditions for recovery for 8-10 days after surgery (LD2) and then released in DD for period determination (DD2). Brains were subsequently recovered to confirm effective SCN targeting and determine Cre recombination rates.

Microscopy

Brains from surgery mice were fixed in 4% PFA, cryo-protected overnight and frozen sections collected at 40 µm on a freezing sledge microtome (Bright Instruments, UK). Successful targeting of the SCN and co-localization of mCherry::Cre and Cry1::EGFP signals were confirmed by immunofluorescence of native EGFP signal (control group), or by mCherry (1:500 Rabbit polyclonal, ab167453 Abcam) and GFP antisera (1:1000, chicken polyclonal, A10262 ThermoFisher) (Cre-treated mice). Other primary antisera used for co-localization studies are: 1:200 rabbit polyclonal anti-Aldh1L1 ab87117 (Abcam); 1:1000 rabbit polyclonal anti-Cx43 C6129 (Sigma) 1:1000 chicken ab13970 polyclonal anti-EGFP (Abcam). Blocking solution 5% normal goat serum. Secondary antisera: goat anti-rabbit conjugated with Alexa 546, goat anti-rabbit conjugated with Alexa 647 and goat anti-chicken conjugated with Alexa 488). Sections were mounted using hard-set medium containing DAPI for nuclear detection (Vectashield). Images were acquired as tiled stacks using a Zeiss 780 confocal microscope (Zeiss), equipped with a 63X oil-immersion objective. Co-localization analysis of GFAP-mCherry::Cre with *Cry1*-Flex-Cry1::EGFP was performed manually on confocal single planes. 1-2 confocal planes were taken into account from in each successfully targeted animal. The procedure was repeated on 5 animals. Number of DAPI+ cells was assessed by the semi-automated nucleus counter plugin of the Fiji Cookbook. SCN

slices in **(Fig. S1)** were fixed and treated as previously described (*3*) and native mCherry::Cre and Cry1::EGFP detected to assess successful Cre-recombination.

Drug treatment

5-(4-Bromophenyl)-3-(1,2-dihydro-6-methyl-2-oxo-4-phenyl-3-quinolinyl)-4,5-dihydro-γ-oxo-1*H*-pyrazole-1-butanoic acid (DQP-1105) and TAT-Gap19 were purchased from Tocris Bioscience; All drugs were diluted in DMSO or ddH2O as required for treatment and corresponding concentration of the dissolving agent used as vehicle controls. For washout, slices were washed 3 times and transferred to fresh medium containing luciferin.

Quantification and statistical analyses

PMT recordings of Per2::Luc^{+} SCN slices from Cry1/2-null mice were filtered by Enright Periodogram to confirm absence of detectable circadian rhythmicity (*27*). Data from PMT recording and imaging data on SCN slices were performed by using the FFT-NLLS function of the online BioDare2 suite (*27*, *28*) (https://biodare2.ed.ac.uk/welcome) (Courtesy of Prof. Andrew Millar, University of Edinburgh) to allow accurate measurement of period, amplitude and relative amplitude error (RAE). Waveform and phase landscape analysis in Fig. 1 were performed as previously described (*3*, *9*). Briefly, Flex-*Cry1*-Luc expressed by GFAP-mCherry::Cre or Syn-mCherry::Cre were collected by long-term live bioluminescence recording (time resolution 0.5 hours) for 3-4 days and de-trended with a 24-hour moving average. The peak-phase of the Syn-GCaMP3 signal co-expressed with Flex-C*ry1*-Luc within each slice was used as an internal marker to phase-align the Flex-*Cry1*-Luc signals in each slice to their respective daily peak of neuronal calcium. To extract the waveform trace, Flex-*Cry1*-Luc and GCaMP3 signal were averaged across 3-4 days within each slice and normalized to reduce stochastic noise. Peak-phase distance between the calcium and the bioluminescence peak was determined manually for each slice. Average waveform traces from 5 independent SCN slices were used to determine the Mean±SEM traces shown in Fig. 1F. Circular statistics to assemble Raleigh plots and compute mean vector lengths for phase-landscape plots was performed by using Oriana 4 (Kovacs Computer Services, UK), as previously described (*3*, *9*). To compare phase data between Cry1/2-null mice and WT mice **(Fig. 3E to K)** phase data from each SCN slice were normalized to the internal periodicity to determine circadian phase. For *in vivo* experiments, emergence of coherent circadian patterns of locomotor activity behavior was assessed by visual inspection and confirmed by using time-frequency analysis (Morlet Continuous Wavelet Transform) in the ClockLab6 suite (ActiMetrics). For accurate period evaluation in DD1 and DD2 windows (detection window= 12 days), data were analyzed by Lomb-Scargle periodogram to compare Cre-treated to control mice. Plots of circadian patterns of locomotor activity were obtained by normalizing locomotor activity to intrinsic periodicity in each mouse and defining activity onset as CT12. To compare data amongst mice with different intrinsic periodicities, data were re-binned to a 0.5h bin size, by averaging intervening values. In all the experiments “n” indicates the number of independent animals/slices analyzed. This information is explicitly reported in figure legend/ texts for each experimental group. ‘‘N’’ refers to the number of cells within a single SCN slice/section. For comparison across different experimental groups statistical significance was assessed with *ad hoc* statistical tests in Prism 6 (GraphPad). The statistical test used, the significance values and the number of experimental replicates for each experimental group is reported in the figure legends. Data were plotted in Prism 6 as Mean±SEM, unless otherwise specified.

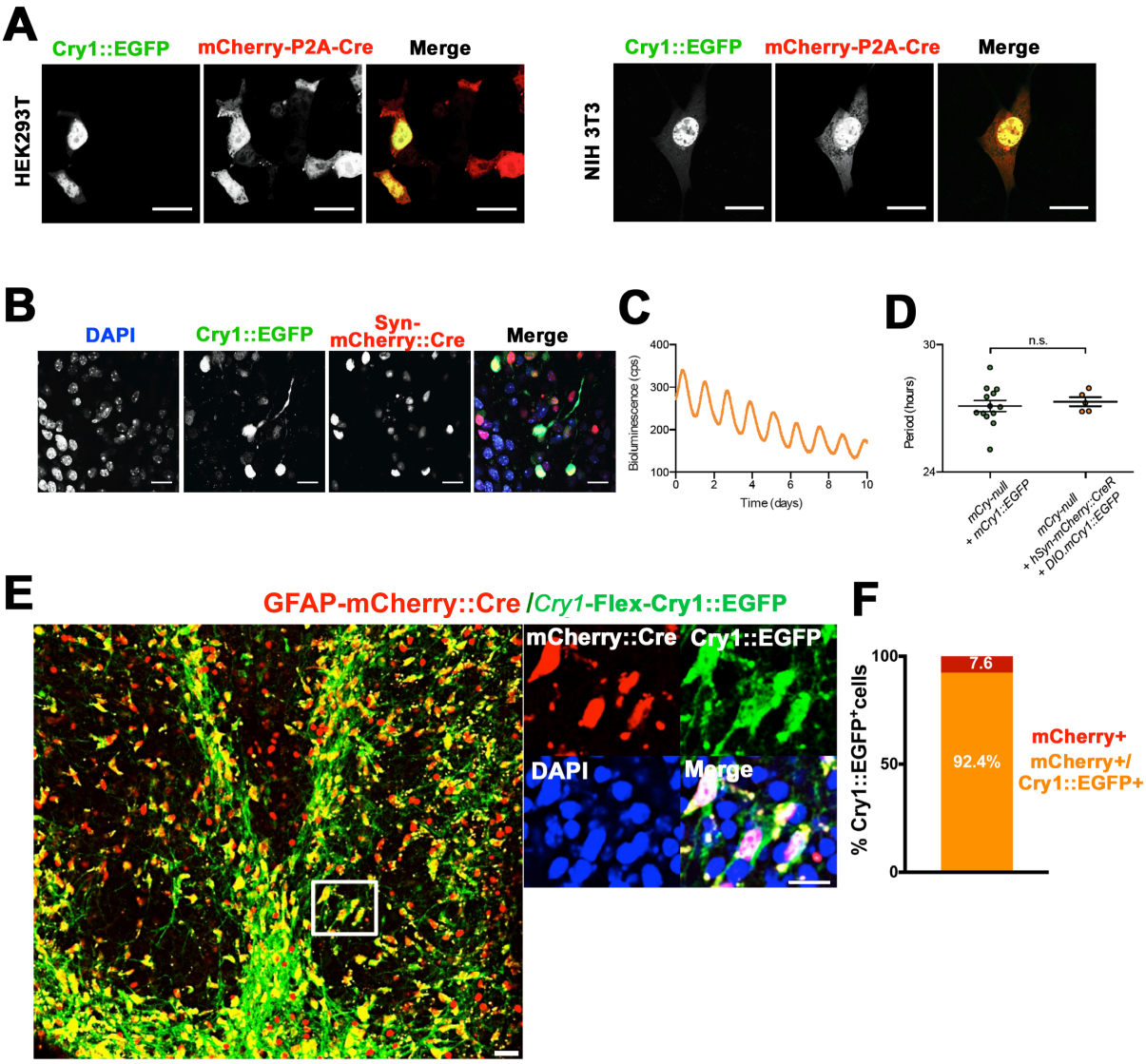

Fig. S1. Validation of Cre-dependent expression of Flex-Cry1::EGFP in targeted cell types.

(A) Confocal micrographs of Cre dependent expression of *Cry1*-Flex-Cry1::EGFP plasmid in HEK293T and NIH3T3 cells on co-transfection with a mCherry-P2A-Cre expressing plasmid. **(B)** Confocal micrographs of *Cry1*-Flex-Cry1::EGFP expression in SCN neurons on co-transduction with Syn-mCherry::Cre AAVs. **(C)** Representative Per2::Luc trace from Cry1/2-null SCN slice co-transduced *Cry1*-Flex-Cry1::EGFP and Syn-mCherry::Cre AAVs. **(D)** Period comparison between Cry1/2-null SCN slices transduced with non-cell-type-specific *Cry1*-Cry1::EGFP (***8***), or *Cry1*-Flex-Cry1::EGFP and Syn-mCherry::Cre (neuronally specific Cry1). **(E)** Confocal microphotograph tile showing Cre-dependent *Cry1*-Flex-Cry1::EGFP expression in SCN slices co-transduced with GFAP-mCherry::Cre (astrocytically specific Cry1 expression). **(F)** Co-localisation relative to (E). $N_{(Cry1::EGFP)}$=630; n=3. Values are Mean±SEM, group size as plotted. **(D)** Statistical test two-tailed t-test. Scale bars: 20µm.

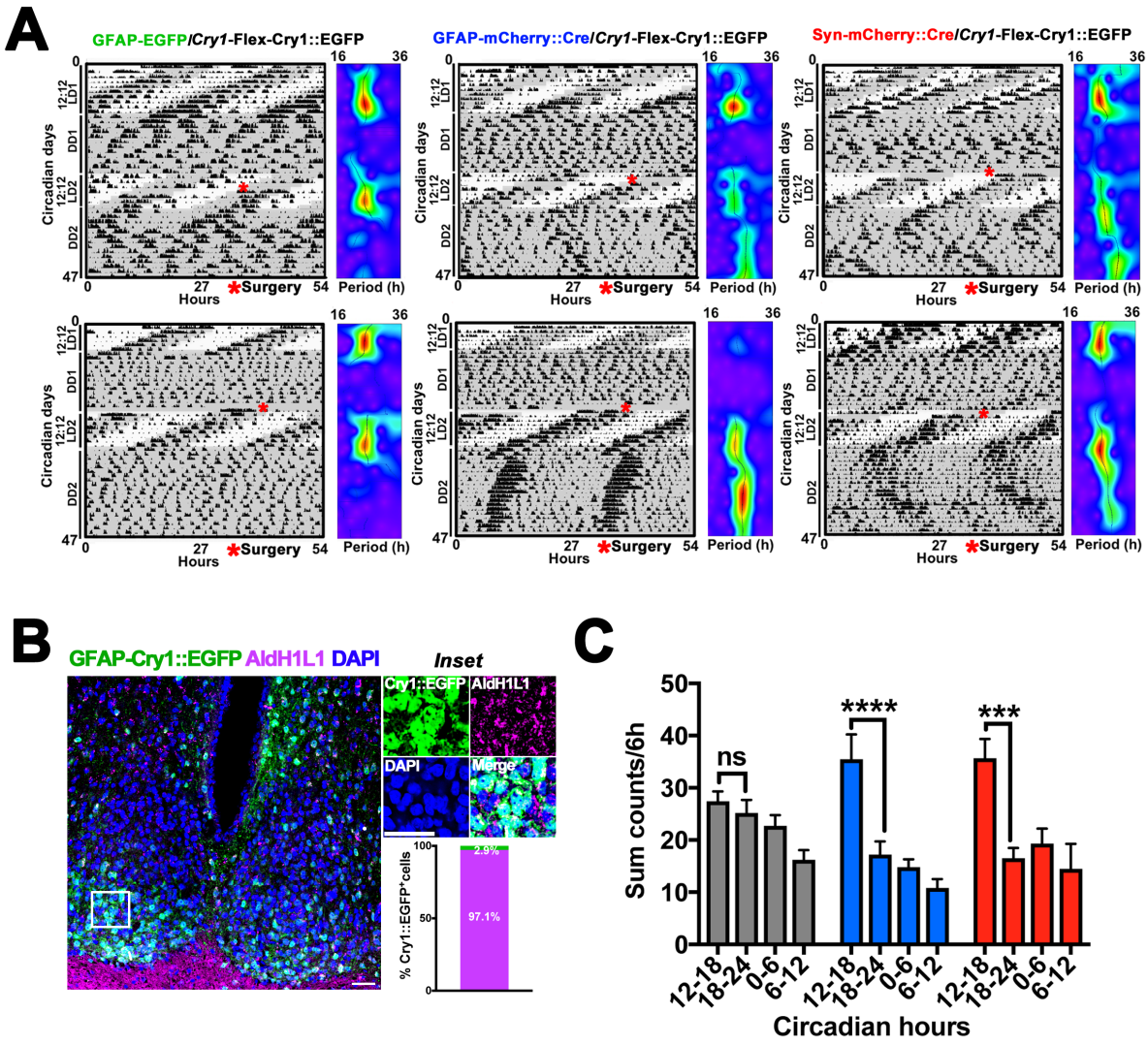

Fig. S2. Astrocytically restricted expression of Cry1 initiates and sustains robust circadian patterns of locomotor activity in adult Cry1/2-null mice- supplement

(A) Additional actograms and wavelet analyses of Cry1/2-null mice targeted with *Cry1*-Flex-Cry1::EGFP together with GFAP-EGFP (control) or Cre expressing AAVs, treated as shown in **Fig. 2.** Rhythmicity in LD1 and 2 is due to masking effect of the light-dark cycle. **(B)** Representative confocal tiled micrograph and histogram for group data showing co-localization of Cry1::EGFP and the astrocytic specific AldH1L1 marker in SCN from Cry1/2-null mice targeted with GFAP-mCherry::Cre and *Cry1*-Flex-Cry1::EGFP. Total number of cells counted $N_{(Cry1::EGFP)}$= 732 from n=4 targeted mice. **(C)** Quantification of circadian locomotor activity plots shown in Fig. 2, summed over 6 circadian hours. Plotted values are Mean±SEM. Group size is $n_{(GFAP-EGFP)}$=7; $n_{(GFAP-Cre)}$=10; $n_{Syn-Cre)}$=5. Statistical test is 2-ways RM-ANOVA, with a Bonferroni correction. ***=p<0.001; ****=p<0.0001. Scale bars= 50 µm.

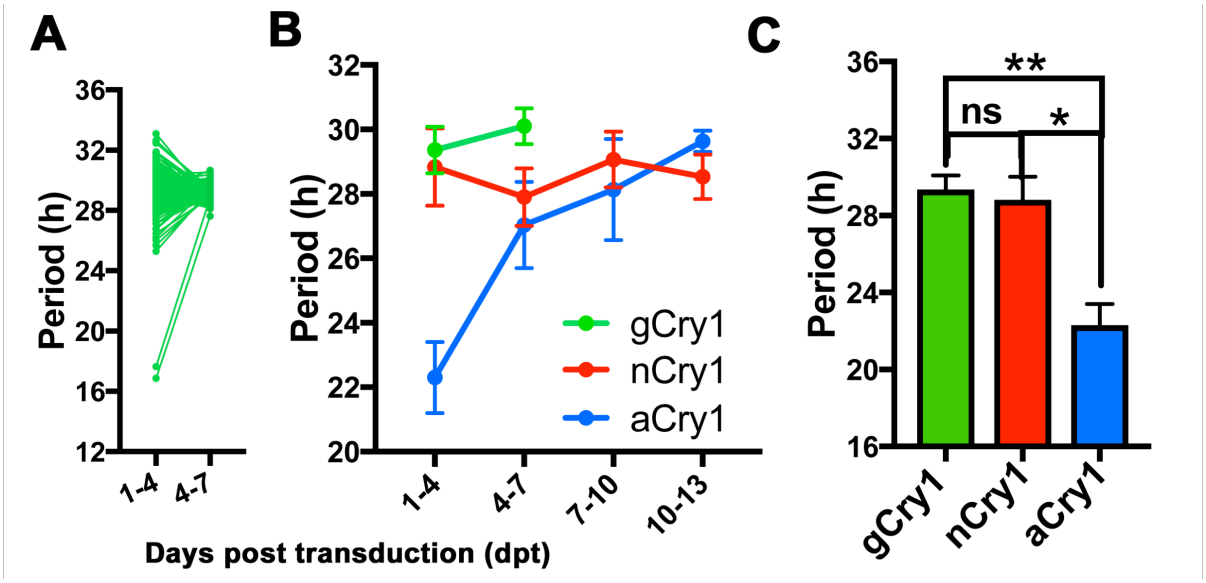

Fig. S3. Comparison of period dynamics upon generalised or cell-type-specific Cry1 expression in Cry1/2-null SCN slices.

(A, B) Representative dynamics of period of Per2::Luc oscillation in Cry1/2-null SCN slices on generalised Cry1 expression (gCry1) (by *Cry1*-Cry::EGFP) in an individual slice (A) and across multiple explants (B). Traces from neuronal and astrocyte-specific Cry1 expression (nCry1 and aCry1) are re-plotted from Fig. 3 for presentational purposes. gCry1 data are re-analysed using the original dataset in (*8*). **(C)** Period comparison of Per2::Luc oscillations on generalised and cell-type specific Cry1 expression in Cry1/2-null SCN slices, showing immediate (dpt 1-4) establishment of 28 hours oscillations in generalised or neuronal, but not astrocytic Cry1 complementation. Mean±SEM. Group size is n=3 for all the groups. Statistical test is ANOVA, with a Bonferroni correction. *=$p<0.05$, **=$p<0.01$.

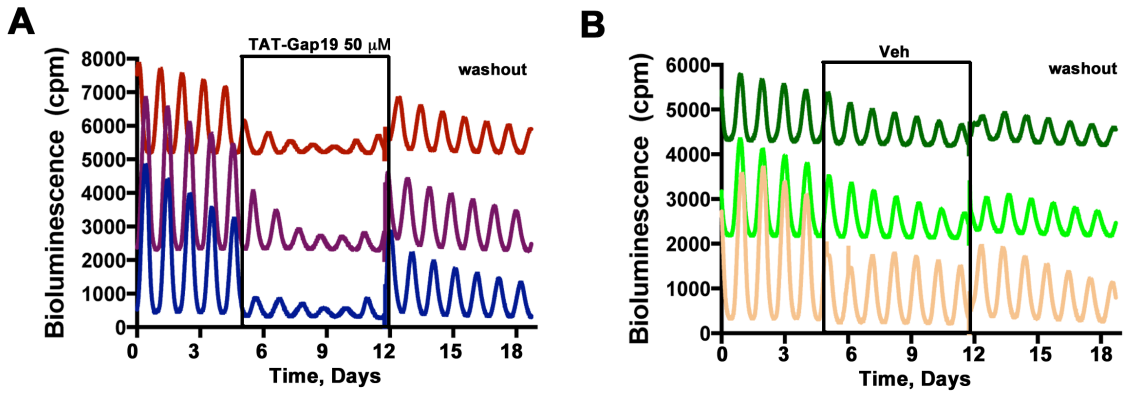

Fig. S4: TAT-Gap19 does not affect viability of SCN slices

(A, B) PMT traces of SCN slices expressing Per2::Luc treated with TAT-Gap19 (50 μM). (A) or vehicle (B), further showing amplitude reduction in the presence of the drug (but not vehicle) and full recovery of the oscillations after washout.

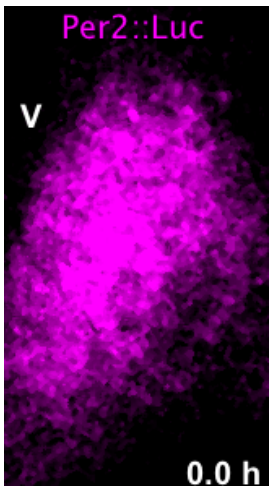

Movie S1

Progressive establishment of Per2::Luc oscillation in Cry1/2-null SCN slices following astrocytically restricted expression of Cry1. Per2::Luc signal from Cry1/2-null SCN slices on astrocytic Cry1 expression (single SCN). The slice had previously been transduced with *Cry1*-Flex-Cry1::EGFP AAV. The recording starts immediately after super-transduction with GFAP-mCherry::Cre AAVs triggering astrocytic specific expression of Cry1. V is third ventricle. Time is hours (h), as indicated in the movie.

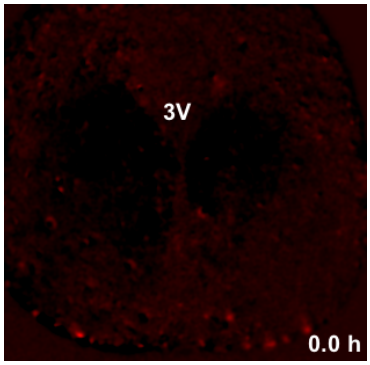

Movie S2

Astrocytically restricted expression of Cry1 fully initiates circadian neuronal activity and spatio-temporal circuit organisation of the SCN in Cry1/2-null mice. Syn-RCaMP1 detecting neuronal intracellular calcium signal from Cry1/2-null SCN slices transduced with *Cry1*-Flex-Cry1::EGFP/ GFAP-mCherry::Cre AAVs to express Cry1 solely in astrocytes. The movie is obtained by subtracting 25 hour moving average to filter noise. 3V is third ventricle. Time is hours (h), as indicated in the movie.

References and Notes

1. M. Koch, A Nobel Pursuit May Not Run like Clockwork. *Cell* **171**, 1246–1251 (2017). doi:10.1016/j.cell.2017.11.030 Medline

2. M. H. Hastings, E. S. Maywood, M. Brancaccio, Generation of circadian rhythms in the suprachiasmatic nucleus. *Nat. Rev. Neurosci.* **19**, 453–469 (2018). doi:10.1038/s41583-018-0026-z Medline

3. M. Brancaccio, A. P. Patton, J. E. Chesham, E. S. Maywood, M. H. Hastings, Astrocytes Control Circadian Timekeeping in the Suprachiasmatic Nucleus via Glutamatergic Signaling. *Neuron* **93**, 1420–1435.e5 (2017). doi:10.1016/j.neuron.2017.02.030 Medline

4. C. F. Tso, T. Simon, A. C. Greenlaw, T. Puri, M. Mieda, E. D. Herzog, Astrocytes Regulate Daily Rhythms in the Suprachiasmatic Nucleus and Behavior. *Curr. Biol.* **27**, 1055–1061 (2017). doi:10.1016/j.cub.2017.02.037 Medline

5. L. M. Prolo, J. S. Takahashi, E. D. Herzog, Circadian rhythm generation and entrainment in astrocytes. *J. Neurosci.* **25**, 404–408 (2005). doi:10.1523/JNEUROSCI.4133-04.2005 Medline

6. J. Livet, T. A. Weissman, H. Kang, R. W. Draft, J. Lu, R. A. Bennis, J. R. Sanes, J. W. Lichtman, Transgenic strategies for combinatorial expression of fluorescent proteins in the nervous system. *Nature* **450**, 56–62 (2007). doi:10.1038/nature06293 Medline

7. J. M. Fustin, J. S. O'Neill, M. H. Hastings, D. G. Hazlerigg, H. Dardente, Cry1 circadian phase in vitro: Wrapped up with an E-box. *J. Biol. Rhythms* **24**, 16–24 (2009). doi:10.1177/0748730408329267 Medline

8. M. D. Edwards, M. Brancaccio, J. E. Chesham, E. S. Maywood, M. H. Hastings, Rhythmic expression of cryptochrome induces the circadian clock of arrhythmic suprachiasmatic nuclei through arginine vasopressin signaling. *Proc. Natl. Acad. Sci. U.S.A.* **113**, 2732–2737 (2016). doi:10.1073/pnas.1519044113 Medline

9. M. Brancaccio, E. S. Maywood, J. E. Chesham, A. S. I. Loudon, M. H. Hastings, A Gq-Ca2+ axis controls circuit-level encoding of circadian time in the suprachiasmatic nucleus. *Neuron* **78**, 714–728 (2013). doi:10.1016/j.neuron.2013.03.011 Medline

10. G. T. J. van der Horst, M. Muijtjens, K. Kobayashi, R. Takano, S. Kanno, M. Takao, J. de Wit, A. Verkerk, A. P. Eker, D. van Leenen, R. Buijs, D. Bootsma, J. H. Hoeijmakers, A. Yasui, Mammalian Cry1 and Cry2 are essential for maintenance of circadian rhythms. *Nature* **398**, 627–630 (1999). doi:10.1038/19323 Medline

11. S.-H. Yoo, S. Yamazaki, P. L. Lowrey, K. Shimomura, C. H. Ko, E. D. Buhr, S. M. Siepka, H.-K. Hong, W. J. Oh, O. J. Yoo, M. Menaker, J. S. Takahashi, PERIOD2::LUCIFERASE real-time reporting of circadian dynamics reveals persistent circadian oscillations in mouse peripheral tissues. *Proc. Natl. Acad. Sci. U.S.A.* **101**, 5339–5346 (2004). doi:10.1073/pnas.0308709101 Medline

12. M. R. Ralph, R. G. Foster, F. C. Davis, M. Menaker, Transplanted suprachiasmatic nucleus determines circadian period. *Science* **247**, 975–978 (1990). doi:10.1126/science.2305266 Medline

13. V. M. King, S. Chahad-Ehlers, S. Shen, A. J. Harmar, E. S. Maywood, M. H. Hastings, A hVIPR transgene as a novel tool for the analysis of circadian function in the mouse suprachiasmatic nucleus. *Eur. J. Neurosci.* **17**, 822–832 (2003). doi:10.1046/j.1460-9568.2003.02487.x

14. N. J. Smyllie, J. E. Chesham, R. Hamnett, E. S. Maywood, M. H. Hastings, Temporally chimeric mice reveal flexibility of circadian period-setting in the suprachiasmatic nucleus. *Proc. Natl. Acad. Sci. U.S.A.* **113**, 3657–3662 (2016). doi:10.1073/pnas.1511351113 Medline

15. M. Brancaccio, R. Enoki, C. N. Mazuski, J. Jones, J. A. Evans, A. Azzi, Network-mediated encoding of circadian time: The suprachiasmatic nucleus (SCN) from genes to neurons to circuits, and back. *J. Neurosci.* **34**, 15192–15199 (2014). doi:10.1523/JNEUROSCI.3233-14.2014 Medline

16. R. Enoki, Y. Oda, M. Mieda, D. Ono, S. Honma, K. I. Honma, Synchronous circadian voltage rhythms with asynchronous calcium rhythms in the suprachiasmatic nucleus. *Proc. Natl. Acad. Sci. U.S.A.* **114**, E2476–E2485 (2017). doi:10.1073/pnas.1616815114 Medline

17. J. Clasadonte, E. Scemes, Z. Wang, D. Boison, P. G. Haydon, Connexin 43-Mediated Astroglial Metabolic Networks Contribute to the Regulation of the Sleep-Wake Cycle. *Neuron* **95**, 1365–1380.e5 (2017). doi:10.1016/j.neuron.2017.08.022 Medline

18. L. C. Mayorquin, A. V. Rodriguez, J.-J. Sutachan, S. L. Albarracín, Connexin-Mediated Functional and Metabolic Coupling Between Astrocytes and Neurons. *Front. Mol. Neurosci.* **11**, 118 (2018). doi:10.3389/fnmol.2018.00118 Medline

19. V. Abudara, J. Bechberger, M. Freitas-Andrade, M. De Bock, N. Wang, G. Bultynck, C. C. Naus, L. Leybaert, C. Giaume, The connexin43 mimetic peptide Gap19 inhibits hemichannels without altering gap junctional communication in astrocytes. *Front. Cell. Neurosci.* **8**, 306 (2014). doi:10.3389/fncel.2014.00306 Medline

20. L. Walrave, A. Pierre, G. Albertini, N. Aourz, D. De Bundel, A. Van Eeckhaut, M. Vinken, C. Giaume, L. Leybaert, I. Smolders, Inhibition of astroglial connexin43 hemichannels with TAT-Gap19 exerts anticonvulsant effects in rodents. *Glia* **66**, 1788–1804 (2018). doi:10.1002/glia.23341 Medline

21. Z.-C. Ye, M. S. Wyeth, S. Baltan-Tekkok, B. R. Ransom, Functional hemichannels in astrocytes: A novel mechanism of glutamate release. *J. Neurosci.* **23**, 3588–3596 (2003). doi:10.1523/JNEUROSCI.23-09-03588.2003 Medline

22. J. S. Marvin, B. G. Borghuis, L. Tian, J. Cichon, M. T. Harnett, J. Akerboom, A. Gordus, S. L. Renninger, T.-W. Chen, C. I. Bargmann, M. B. Orger, E. R. Schreiter, J. B. Demb, W.-B. Gan, S. A. Hires, L. L. Looger, An optimized fluorescent probe for visualizing glutamate neurotransmission. *Nat. Methods* **10**, 162–170 (2013). doi:10.1038/nmeth.2333 Medline

23. T. M. Acker, H. Yuan, K. B. Hansen, K. M. Vance, K. K. Ogden, H. S. Jensen, P. B. Burger, P. Mullasseril, J. P. Snyder, D. C. Liotta, S. F. Traynelis, Mechanism for noncompetitive inhibition by novel GluN2C/D N-methyl-D-aspartate receptor subunit-selective modulators. *Mol. Pharmacol.* **80**, 782–795 (2011). doi:10.1124/mol.111.073239 Medline

24. J. F. Oliveira, V. M. Sardinha, S. Guerra-Gomes, A. Araque, N. Sousa, Do stars govern our actions? Astrocyte involvement in rodent behavior. *Trends Neurosci.* **38**, 535–549 (2015). doi:10.1016/j.tins.2015.07.006 Medline

25. T. Papouin, J. M. Dunphy, M. Tolman, K. T. Dineley, P. G. Haydon, Septal Cholinergic Neuromodulation Tunes the Astrocyte-Dependent Gating of Hippocampal NMDA Receptors to Wakefulness. *Neuron* **94**, 840–854.e7 (2017). doi:10.1016/j.neuron.2017.04.021 Medline

26. M. Martin-Fernandez, S. Jamison, L. M. Robin, Z. Zhao, E. D. Martin, J. Aguilar, M. A. Benneyworth, G. Marsicano, A. Araque, Synapse-specific astrocyte gating of amygdala-related behavior. *Nat. Neurosci.* **20**, 1540–1548 (2017). doi:10.1038/nn.4649 Medline

27. T. Zielinski, A. M. Moore, E. Troup, K. J. Halliday, A. J. Millar, Strengths and limitations of period estimation methods for circadian data. *PLOS ONE* **9**, e96462 (2014). doi:10.1371/journal.pone.0096462 Medline

28. A. Moore, T. Zielinski, A. J. Millar, Online period estimation and determination of rhythmicity in circadian data, using the BioDare data infrastructure. *Methods Mol. Biol.* **1158**, 13–44 (2014). doi:10.1007/978-1-4939-0700-7_2 Medline